Supporting Information

# Halogen-Bonded Ionic Liquid Crystals: Supramolecular Organization and Ionic Transport

*Mercedes Marcos,[a,b] Alberto Concellón,[a,b] Almudena Terrel,[a,b] Rosa I. Merino,[a,c] Rosa M. Tejedor,[d] Joaquín Barberá,[a,b] José L. Serrano, [a,b,]* and Santiago Uriel[a,b,]**

[a] Instituto de Nanociencia y Materiales de Aragón (INMA), CSIC-Universidad de Zaragoza, 50009 Zaragoza, Spain.
[b] Departamento de Química Orgánica, Universidad de Zaragoza, 50009 Zaragoza, Spain.
[c] Departamento de Física de la Materia Condensada, Universidad de Zaragoza, 50009 Zaragoza, Spain.
[d] Centro Universitario de la Defensa Academia General Militar, Zaragoza, Spain.

* To whom correspondence should be addressed: joseluis@unizar.es (J.L.S), suriel@unizar.es (S.U)

# Contents

# 1 MATERIALS AND METHODS

## 1.1 General information

All commercially available reagents were purchased and used without further purification. Nuclear magnetic resonance (NMR) spectra were recorded on Bruker Avance 400 spectrometer (9.4T, 400.13 MHz for $^{1}H$, 100.62 MHz for $^{13}C$). $^{1}H$ and $^{13}C$ chemical shifts (δ) are reported in ppm relative to tetramethylsilane, using solvent residual signals as the references: $CDCl_3$ (7.26 ppm for $^{1}H$ NMR and 77.0 ppm for $^{13}C$ NMR). MS-ESI spectra were obtained on an ESQUIRE 3000plus (Bruker Daltonics) spectrometer. The mesophase identification was based on microscopic examination of the textures formed by samples between two glass plates. NIKON and OLYMPUS BH–2 polarizing microscopes equipped with a LINKAM THMS600 hot stage were used. The temperatures and enthalpies of the phase transitions were determined by calorimetric measurements performed with DSC TA Instrument Q–20 and Q–2000 systems. Thermogravimetric analysis (TGA) was performed using a TA Q5000IR instrument at a heating rate of 10 ºC /min under a nitrogen atmosphere. The X–ray investigations on non–oriented samples were carried out in Lindemann capillary tubes (diameter: 0.9 or 1 mm) using a PINHOLE (ANTON–PAAR) film camera.

## 1.2 General procedure for preparation of 1-alkyl-3-halopyridinium halides

3-Halopyridine (2.0 mmol) and corresponding haloalkane (2.4 mmol,) were heated in 10 mL of dried toluene for 20 h at 100–110 ºC. After cooling to room temperature, the crude product was purified by washing with diethyl ether to give the 1-alkyl-3-halopyridinium halide with a yield ranged from 60 to 85%.

## 1.3 Characterization of 1-alkyl-3-halopyridinium halides

**1-Decyl-3-bromopyridinium bromide (Py-Br-Br-10)**

$^{1}H$ NMR (DMSO-d$^{6}$, J/Hz) δ = 9.78 (s, 1 H, Ar-H), 9.38 (1 H, Ar-H), 8.88 (1 H, Ar-H), 8.11 (1 H, Ar-H), 4.68 (t, *J* = 7.4 Hz, 2 H, $CH_2$), 1.87 (m, 2 H, $CH_2$), 1.27-1.11 (m, 14 H, $CH_2$), 0.79 (t, *J* = 6.9 Hz, 3 H, $CH_3$).

$^{13}C$ NMR (DMSO-d$^{6}$) δ =.147.96, 146.16, 144,23, 129.01, 122.10, 60.79, 31.37, 30.89, 28.98, 28.89, 28.75, 28.53, 25.45, 22.20, 14.11

HR-MS (ESI$^{+}$, $CH_3CN$) found: m/z = 298.1174 $[M]^{+}$ (298.1165 calc. for $C_{15}H_{25}BrN^{+}$), 677.1478 $[2M{\cdot}Br]^{+}$; (677.1500 calc. for $C_{30}H_{50}Br_3N_2^{+}$)

HR-MS (ESI$^{-}$, $CH_3CN$) found: m/z = 457.9471 $[M{\cdot}2Br]^{-}$ (457.9539 calc. for $C_{15}H_{25}Br_3N^{-}$)

**1-Decyl-3-iodopyridinium bromide (Py-I-Br-10)**

$^{1}H$ NMR (DMSO-d$^{6}$, J/Hz) δ = 9.61 (s, 1 H, Ar-H), 9.31 (1 H, Ar-H), 8.90 (1 H, Ar-H), 7.90 (1 H, Ar-H), 4.61 (t, *J* = 7.4 Hz, 2 H, $CH_2$), 1.84 (m, 2 H, $CH_2$), 1.27-1.11 (m, 14 H, $CH_2$), 0.79 (t, *J* = 6.9 Hz, 3 H, $CH_3$).

$^{13}C$ NMR (DMSO-d$^{6}$) δ =.152.88, 149.78, 143.76, 128.70, 99.26, 60.43, 31.37, 30.94, 28.96, 28.88, 28.73, 28.50, 25.47, 22.20, 14.11

HR-MS (ESI$^+$, $CH_3CN$) found: m/z = 346.0955 [M]$^+$ (346.1026 calc. for $C_{15}H_{25}IN^+$), 773.1257 [2M·Br]$^+$; (773.1222 calc. for $C_{30}H_{50}I_2N_2Br^+$)
MS (ESI$^-$, $CH_3CN$) found: m/z = 505.9406 [M·2Br]$^-$ (505.9373 calc. for $C_{15}H_{25}INBr_2^-$)

**1-Dodecyl-3-bromopyridinium bromide (Py-Br-Br-12)**
$^1$H NMR (DMSO-d$^6$, J/Hz) δ = 9.78 (s, 1 H, Ar-H), 9.38 (1 H, Ar-H), 8.88 (1 H, Ar-H), 8.11 (1 H, Ar-H), 4.68 (t, *J* = 7.4 Hz, 2 H, $CH_2$), 1.87 (m, 2 H, $CH_2$), 1.27-1.11 (m, 18 H, $CH_2$), 0.79 (t, *J* = 6.9 Hz, 3 H, $CH_3$).
$^{13}$C NMR (DMSO-d$^6$) δ =.147.96, 146.15, 144.22, 129.01, 122.09, 60.80, 31.38, 30.89, 29.09, 29.02, 28.89, 28.79, 28.53, 25.46, 22.20,14.10
HR-MS (ESI$^+$, $CH_3CN$) found: m/z = 326.1488 [M]$^+$ (326.1478 calc. for $C_{17}H_{29}BrN^+$), 733.1976 [2M·Br]$^+$; (733.2126 calc. for $C_{34}H_{58}Br_3N_2^+$)
HR-MS (ESI$^-$, $CH_3CN$) found: m/z = 485.9809 [M·2Br]$^-$ (485.9825 calc. for $C_{17}H_{29}Br_3N^-$)

**1-Dodecyl-3-iodopyridinium bromide (Py-I-Br-12)**
$^1$H NMR (DMSO-d$^6$, J/Hz) δ = 9.61 (s, 1 H, Ar-H), 9.31 (1 H, Ar-H), 8.90 (1 H, Ar-H), 7.90 (1 H, Ar-H), 4.61 (t, 2 H, $CH_2$), 1.84 (m, 2 H, $CH_2$), 1.17 (m, 18 H, $CH_2$), 0.79 (t, 3 H, $CH_3$).
$^{13}$C NMR (DMSO-d$^6$) δ =.152.89, 149.77, 143.75, 128.72, 99.25, 60.47, 31.37, 30.95, 29.09, 29.00, 28.88, 28.79, 28.50, 25.47, 22.23, 14.11
HR-MS (ESI$^+$, $CH_3CN$) found: m/z = 374.1316 [M]$^+$ (374.1339 calc. for $C_{17}H_{29}IN^+$), 827.1813 [2M·Br]$^+$; (827.1867 calc. for $C_{34}H_{58}I_2BrN_2^+$)
HR-MS (ESI$^-$, $CH_3CN$) found: m/z = 533.9703 [M·2Br]$^-$ (533.9686 calc. for $C_{17}H_{29}Br_2IN^-$)

**1-Tetradecyl-3-bromopyridinium bromide (Py-Br-Br-14)**
$^1$H NMR (DMSO-d$^6$, J/Hz, 400 MHz) δ = 9.78 (s, 1 H, Ar-H), 9.38 (1 H, Ar-H), 8.88 (1 H, Ar-H), 8.11 (1 H, Ar-H), 4.68 (t, *J* = 7.45 Hz, 2 H, $CH_2$), 1.87 (m, 2 H, $CH_2$), 1.27-1.11 (m, 22 H, $CH_2$), 0.79 (t, *J* = 7.1 Hz, 3 H, $CH_3$).
$^{13}$C NMR (DMSO-d$^6$) δ = 147.96, 146.16, 144.22, 129.00, 122.10, 60.79, 31.38, 30.90, 29.15, 29.03, 28.90, 28.79, 28.54, 25.46, 22.20, 14.11.
MS (ESI$^-$, $CH_3CN$) found: m/z = 515.8 [M$^+$·2Br$^-$]$^-$ (516.0 calc. for $(C_{19}H_{33}Br_3N)^-$)

**1-Tetradecyl-3-bromopyridinium iodide (Py-Br-I-14)**
$^1$H NMR (DMSO-d$^6$, *J*/Hz) δ = 9.51 (s, 1 H, Ar-H), 9.12 (m, 1 H, Ar-H), 8.87 (m, 1 H, Ar-H), 8.12 (m, 1 H, Ar-H), 4.56 (t, *J* = 7.4 Hz, 2 H, $CH_2$), 1.92 (m, 2 H, $CH_2$), 1.34-1.17 (m, 22 H, $CH_2$), 0.85 (t, *J* = 6.9 Hz, 3 H, $CH_3$).
$^{13}$C NMR (DMSO-d$^6$) δ =.147.79, 145.99, 143.80, 128.81, 122.08, 61.13, 31.27, 30.53, 29.04, 29.01, 28.99, 28.98, 28.89, 28.73, 28.69, 28.35, 25.36, 22.07, 13.94.
MS (ESI$^-$, $CH_3CN$) found: m/z = 609.7 [M$^+$·2I$^-$]$^-$ (610.0 calc. for $(C_{19}H_{33}BrI_2N)^-$)

**1-Tetradecyl-3-iodopyridinium bromide (Py-I-Br-14)**
$^1$H NMR (DMSO-d$^6$, J/Hz) δ = 9.50 (s, 1 H, Ar-H), 9.12 (1 H, Ar-H), 8.94 (1 H, Ar-H), 7.93 (1 H, Ar-H), 4.52 (2 H, $CH_2$), 1.90 (m, 2 H, $CH_2$), 1.27-1.11 (m, 22 H, $CH_2$), 0.84 (3 H, $CH_3$).

$^{13}C$ NMR (DMSO-d$^6$) δ =.152.85, 149.88, 143.70, 128.62, 96.40, 60.73, 31.28, 30.68, 29.03, 28.98, 28.88, 28.75, 28.70, 28.33, 25.36, 22.08, 13.94
HR-MS (ESI$^+$, $CH_3CN$) found: m/z = 402.1705 $[M]^+$ (402.1652 calc. for $C_{19}H_{33}IN^+$), 885.2382 $[2M\cdot Br]^+$; (885.2475 calc. for $C_{38}H_{66}I_2N_2Br^+$)
HR-MS (ESI$^-$, $CH_3CN$) found: m/z=561.9980 $[M\cdot 2Br]^-$ (561.9999 calc. for $C_{19}H_{33}IBr_2N^-$)

**1-Tetradecyl-3-iodopyridinium iodide (Py-I-I-14)**
$^1H$ NMR (DMSO-d$^6$, J/Hz) δ = 9.48 (s, 1 H, Ar-H), 9.10 (m, 1 H, Ar-H), 8.96 (m, 1 H, Ar-H), 7.93 (m, 1 H, Ar-H), 4.52 (t, *J* = 7.4 Hz, 2 H, $CH_2$), 1.90 (m, 2 H, $CH_2$), 1.33-1.16 (m, 22 H, $CH_2$), 0.85 (t, *J* = 6.9 Hz, 3 H, $CH_3$).
$^{13}C$ NMR (DMSO-d$^6$) δ =.152.92, 149.86, 143.65, 128.56, 90.05, 60.78, 31.25, 30.56, 29.02, 29.00, 28.97, 28.95, 28.87, 28.71, 28.66, 28.31, 25.35,22.05,13.92.
HR-MS (ESI$^+$, $CH_3CN$) found: m/z = 402.1656 $[M]^+$ (402.1645 calc. for $C_{19}H_{33}IN^+$), 931.2045 $[2M\cdot I]^+$; (931.2355 calc. for $C_{38}H_{66}I_3N_2^+$)
HR-MS (ESI$^-$, $CH_3CN$) found: m/z = 655.9664 $[M\cdot 2I]^-$ (655.9742 calc. for $C_{19}H_{33}I_3N^-$)

**1-Octadecyl-3-bromopyridinium bromide (Py-Br-Br-18)**
$^1H$ NMR (DMSO-d$^6$, J/Hz) δ = 9.50 (s, 1 H, Ar-H), 9.11 (1 H, Ar-H), 8.86 (1 H, Ar-H), 8.09 (1 H, Ar-H), 4.55 (2 H, $CH_2$), 1.90 (2 H, $CH_2$), 1.26-1.19 (30 H, $CH_2$), 0.85 (3 H, $CH_3$).
$^{13}C$ NMR (DMSO-d$^6$) δ =.147.86, 146.03, 143.87, 128.86, 122.13, 61.22, 31.32, 30.59, 29.06, 29.02, 28.95, 28.79, 28.72, 28.41, , 25.41, 22.13, 13.99.
HR-MS (ESI$^+$, $CH_3CN$) found: m/z = 410.2434 $[M]^+$ (410.2417 calc. for $C_{23}H_{41}BrN^+$),
MS (ESI$^-$, $CH_3CN$) found: m/z = 571.8 $[M^+\cdot 2Br^-]^-$ (572.1 calc. for $(C_{23}H_{41}Br_3N)^-$)

**1-Octadecyl-3-bromopyridinium iodide (Py-Br-I-18)**
$^1H$ NMR (DMSO-d$^6$, J/Hz) δ = 9.51 (s, 1 H, Ar-H), 9.12 (1 H, Ar-H), 8.88 (1 H, Ar-H), 8.11 (1 H, Ar-H), 4.56 (t, *J* = 7.4 Hz, 2 H, $CH_2$), 1.92(m, 2 H, $CH_2$), 1.33-1.16 (m, 14 H, $CH_2$), 0.85 (t, *J* = 6.9 Hz, 3 H, $CH_3$).
$^{13}C$ NMR (DMSO-d$^6$) δ =.147.78, 145.97, 143.78, 128.79, 122.06, 61.12, 31.25, 30.51, 29.00, 28.96, 28.88, 28.72, 28.66, 28.34, 25.35, 22.05, 13.92.
MS (ESI$^-$, $CH_3CN$) found: m/z = 663.9 $[M^+\cdot 2I^-]^-$ (664.1 calc. for $(C_{23}H_{41}BrI_2N)^-$)
MS (ESI$^+$, $CH_3CN$) found: m/z = 410.4 $[M]^+$ (410.2 calc. for $(C_{23}H_{41}BrN)^+$)

**1-Octadecyl-3-iodopyridinium bromide (Py-I-Br-18)**
$^1H$ NMR (DMSO-d$^6$, J/Hz) δ = 9.61 (1 H, Ar-H), 9.31 (1 H, Ar-H), 8.89 (1 H, Ar-H), 7.90 (1 H, Ar-H), 4.61 (2 H, $CH_2$), 2.15 (2 H, $CH_2$), 1.27-1.10 (30 H, $CH_2$), 0.78 (3 H, $CH_3$).
$^{13}C$ NMR (DMSO-d$^6$) δ =.152.94, 149.89, 143.68, 128.56, 96.06, 60.76, 31.28, 30.61, 29.02, 28.98, 28.90, 28.74, 28.68, 28.35, 25.38, 22.08, 13.95.
HR-MS (ESI$^+$, $CH_3CN$) found: m/z = 458.2265 $[M]^+$ (458.2278 calc. for $C_{23}H_{41}IN^+$)

**1-Octadecyl-3-iodopyridinium iodide (Py-I-I-18)**

$^1$H NMR (DMSO-d$^6$, J/Hz) δ = 9.48 (s, 1 H, Ar-H), 9.09 (1 H, Ar-H), 8.96 (1 H, Ar-H), 7.92 (1 H, Ar-H), 4.51 (t, *J* = 7.5 Hz, 2 H, $CH_2$), 1.9 (m, 2 H, $CH_2$), 1.32-1.18 (m, 30 H, $CH_2$), 0.85 (t, *J* = 6.9 Hz, 3 H, $CH_3$).

HR-MS (ESI$^-$, $CH_3CN$) found: m/z=711.9766 $[M^+ \cdot 2I^-]^-$ (712.0368 calc. for $(C_{23}H_{41}I_3N)^-$)

HR-MS (ESI$^+$, $CH_3CN$) found: m/z=458.2253 $[M]^+$ (458.2278 calc. for $(C_{23}H_{41}IN)^+$)

# 2 X-RAY MONOCRYSTAL DIFFRACTION

## 2.1 General procedure

X-Ray diffraction experiments were carried out on Agilent/Rigaku, SuperNova Mo and Agilent/Rigaku, SuperNova Dual diffractometers. Software packages XSCANS[1] and CrysAlisPro[2] were used to process data. Final cell parameters were obtained by global refinement of reflections obtained from integration of all the frames data. The structures were solved by direct methods and refined by the full-matrix method based on F2 using SHELXL program.[3] The non-hydrogen atoms were refined anisotropically. The hydrogen atoms were observed in difference electron density maps or included at idealized positions by using a riding model and refined isotropically.

The crystal parameters and basic information relating data collection and structure refinement for the compounds are summarized in Table S1

## 2.2 Tables

**Table S1.** General and crystallographic parameters for **Py−I−Br−10, Py−I−Br−12 and Py−I−Br−18**

| | **Py-I-Br-10** | **Py-I-Br-12** | **Py-I-Br-18** |
|---|---|---|---|
| **Emp. formula** | $C_{15}H_{25}BrIN$ | $C_{17}H_{29}BrIN$ | $C_{23}H_{41}BrIN$ |
| **Formula weight** | 426.17 | 454.22 | 538.38 |
| **Crystal system** | Monoclinic | Monoclinic | Triclinic |
| **a, Å** | 14.3482(7) | 14.6186(6) | 7.9566(9) |
| **b, Å** | 15.3153(9) | 51.5551(18) | 10.6160(7) |
| **c, Å** | 16.1789(13) | 15.9767(6) | 31.0148(12) |
| **α, deg** | | | 85.442(4) |
| **β, deg** | 103.111(6) | 99.182(4) | 83.365(6) |
| **γ , deg** | | | 78.292(8) |
| **Volume, Å$^3$** | 3462.6(4) | 11886.8(8) | 2543.8(4) |
| **T, K** | 150(2) | 150(2) | 150(2) |
| **Space group** | $P2_1/c$ | I2/a | P-1 |
| **Z** | 8 | 4 | 4 |
| **μ(X Kα), mm$^{-1}$** | 4.144 | 14.985 | 11.757 |
| **θ range, deg** | 3.165- 23.255 | 3.429- 65.078 | 4.26- 66.495 |
| **Refl. collected** | 14809 | 10159 | 16080 |
| **Uniq reflect/ Rint** | 4950/0.0922 | 7599/0.0933 | 5585/ 0.1012 |
| **R1/wR2 [I>2σ]** | 0.0599/ 0.0756 | 0.0596/0.1571 | 0.1331/0.3353 |
| **R1/wR2 (all data)** | 0.1156/ 0.0982 | 0.0801/0.1879 | 0.1779/0.3803 |
| **Residual ρ/ e Å$^{-3}$** | 1.309/-0.740 | 1.621/-1.423 | 5.103/-2.017 |

**Table S2**. Geometrical features of the halogen bond interactions in the crystal structures **Py−I−Br−10**, **Py−I−Br−12** and **Py−I−Br−18**.

| Compound | $C–X_1...X_2^-$ | Sym. equivalence | $d(C–X_1)$ Å | $d(X_1...X_2^-)$ Å | $<(CX_1X_2)$ º | *rr*[a] |
|---|---|---|---|---|---|---|
| **Py−I−Br−10** | C(2)−I(1)···Br(1) | x, y, z | 2.11 | 3.339 | 172.9 | 0.85 |
| | C(22)−I(20)···Br(2) | x, y, z | 2.11 | 3.1978 | 176.3 | 0.81 |
| **Py−I−Br−12** | C(2)−I(1)···Br(2) | x, y, z | 2.109 | 3.292 | 177.9 | 0.84 |
| | C(22)−I(20)···Br(4) | -½+x, 1-y, z | 2.097 | 3.3081 | 169.5 | 0.84 |
| | C(42)−I(40)···Br(1) | x, y, z | 2.095 | 3.402 | 170.0 | 0.86 |
| **Py−I−Br−18** | C(2)−I(1)···Br(1) | 1+x, -1+y, z | 2.10 | 3.222 | 179.1 | 0.82 |
| | C(32)−I(30)···Br(1) | 1-x, 1-y, -z | 2.11 | 3.261 | 172.4 | 0.83 |

[a] Reduction ratio, $rr = d(I...X_2^-)/(RvdW(I) + Rionic(X_2^-))$ where RvdW(I) is the van der Waals radii of iodine (1.98 Å) and $Rionic(X_2^-)$ is the Pauling ionic radius of bromide (1.95 Å).

**Table S3**. Hydrogen bond distances and angles in **Py−I−Br−10, Py−I−Br−12, Py−I−Br−18 Py−I−I−14** and **Py−I−I−18**.

| Compound | D-H···A | Sym. equivalence | d(D-H) Å | d(H···A) Å | d(D···A) Å | <(DHA) º |
|---|---|---|---|---|---|---|
| **Py−I−Br−10** | C(1)-H···Br(2) | -1+x, y, z | 0.93 | 2.778 | 3.649 | 156.6 |
| | C(6)-H···Br(2) | -1+x, y, z | 0.97 | 2.984 | 3.857 | 150.3 |
| | C(5)-H···Br(1) | -x, ½+y, ½-z | 0.93 | 2.835 | 3.721 | 159.9 |
| | C(4)-H···Br(2) | 1-x, ½+y, ½-z | 0.93 | 2.851 | 3.57 | 135.5 |
| | C(24)-H···Br(2) | x, ½-y, ½+z | 0.93 | 3.045 | 3.646 | 123.8 |
| | C(23)-H···Br(2) | x, ½-y, ½+z | 0.93 | 2.934 | 3.599 | 129.7 |
| | C(21)-H···Br(1) | x, y, z | 0.93 | 3.029 | 3.880 | 152.8 |
| | C(25)-H···Br(1) | x, ½-y, ½+z | 0.93 | 2.747 | 3.670 | 175.6 |
| **Py−I−Br−12** | C(1)-H···Br(1) | x, y, z | 0.93 | 2.731 | 3.597 | 155.3 |
| | C(6)-H···Br(1) | x, y, z | 0.97 | 2.929 | 3.844 | 157.6 |
| | C(23)-H···Br(3) | x, y, z | 0.93 | 2.985 | 3.630 | 127.9 |
| | C(25)-H···Br(4) | x, y, z | 0.93 | 3.020 | 3.624 | 124.0 |
| **Py−I−Br−18** | C(1)-H···Br(2) | x, y, z | 0.93 | 2.907 | 3.76 | 153 |
| | C(3)-H···Br(1) | x, 1-y, z | 0.93 | 2.880 | 3.58 | 134 |
| | C(17)-H···Br(2) | x, y, z | 0.97 | 2.916 | 3.80 | 152 |
| | C(6)-H···Br(2) | x, y, z | 0.97 | 2.844 | 3.77 | 160 |
| | C(33)-H···Br(1) | -x, 1-y, -z | 0.95 | 2.901 | 3.56 | 129 |
| | C(36)-H···Br(1) | x, y, z | 0.97 | 2.994 | 3.85 | 149 |

**Table S4**. Angles formed by the alkyl chain and the pyridinium plane in crystal structures of **Py−I−Br−10**, **Py−I−Br−12** and **Py−I−Br−18**.

| **Compound** | Angle (º) |
|---|---|
| **Py−I−Br−10** | 133.2 |
| | 106.8 |
| **Py−I−Br−12** | 153.5 |
| | 143.8 |
| | 92.4 |
| **Py−I−Br−18** | 155.0 |
| | 146.4 |
| **Py−I−I−14** | 103.0 |
| **Py−I−I−18** | 103.0 |

## 2.3 Figures

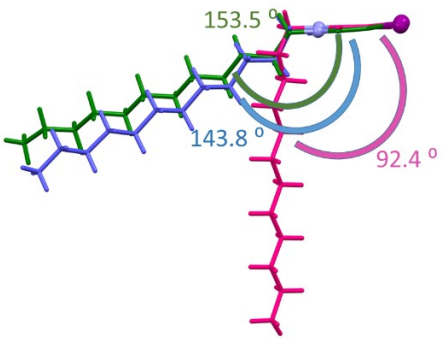


**Figure S1**. Conformation of three crystallographically independent cations in **Py−I−Br−12** crystal structure.

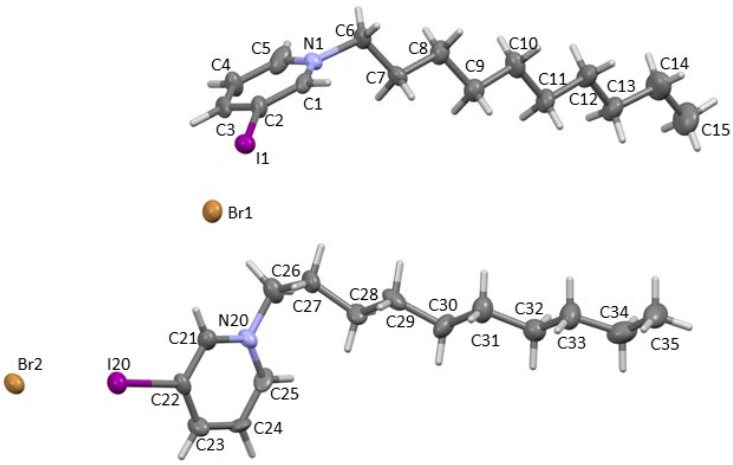


**Figure S2**. ORTEP diagram of asymmetric unit of **Py−I−Br−10** crystal structure showing the atom numbering scheme. Ellipsoid probability level is 50%.

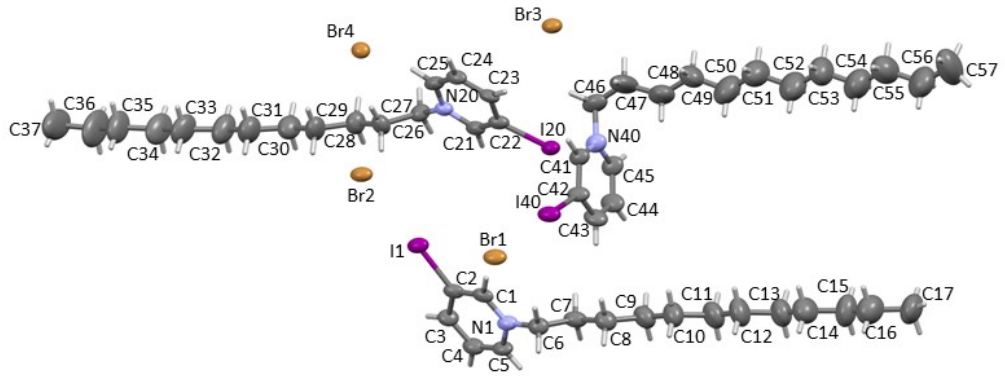


**Figure S2**. ORTEP diagram of asymmetric unit of **Py−I−Br−12** crystal structure showing the atom numbering scheme. Ellipsoid probability level is 50%.

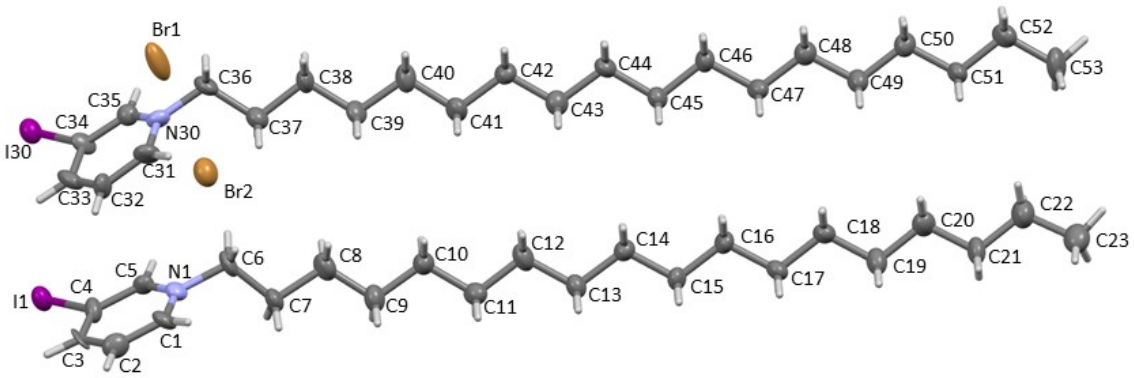


**Figure S3**. ORTEP diagram of asymmetric unit of **Py−I−Br−18** crystal structure showing the atom numbering scheme. Ellipsoid probability level is 50%.

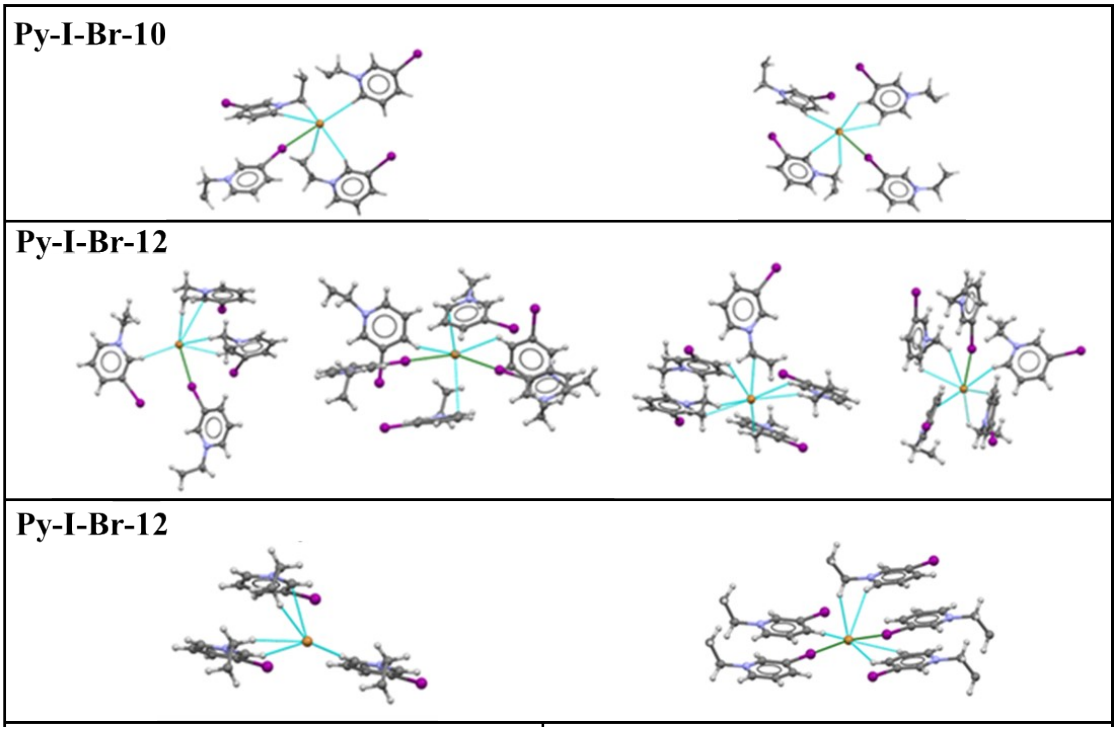


**Figure S4**. Halide anion coordination sphere in crystal structures **Py−I−Br−10, Py−I−Br−12** and **Py−I−Br−18**. Hydrogen bonds are shown in blue, halogen bonds in green and $\pi\cdots I^-$ interactions in orange.

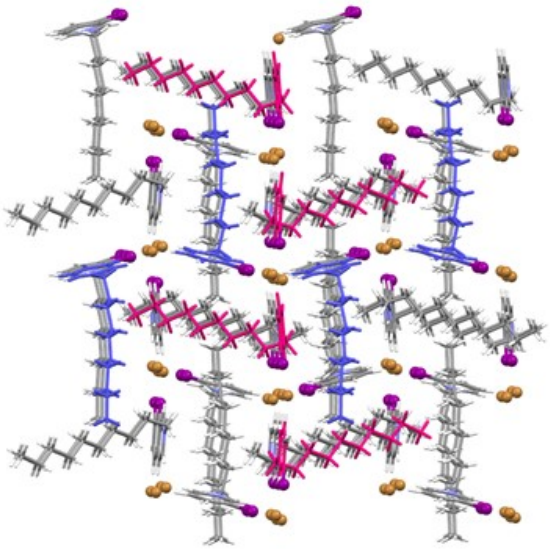

**Figure S5**. Packing diagram of **Py−I−Br−10** crystal structure. The two crystallographically independent cations are shown in blue and red.

# 3 NMR SPECTRA

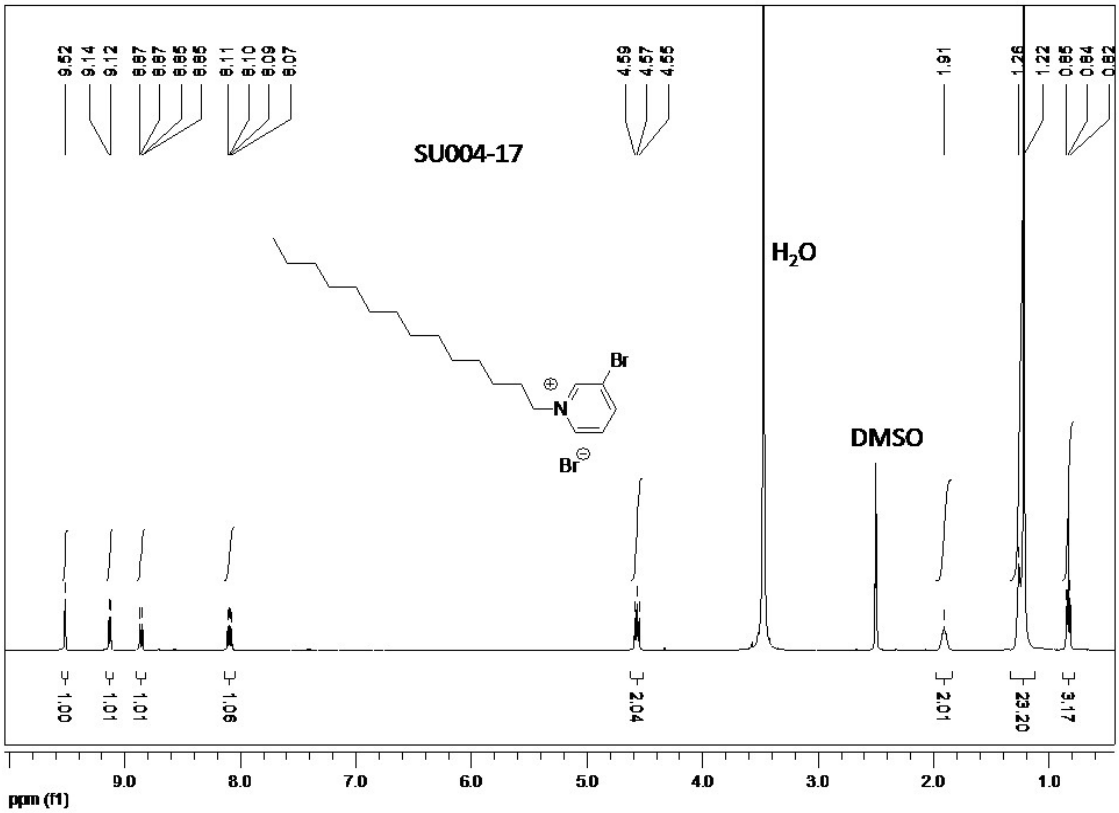


**Figure S6**. [1]H-NMR spectrum of **Py-Br-Br-14**.

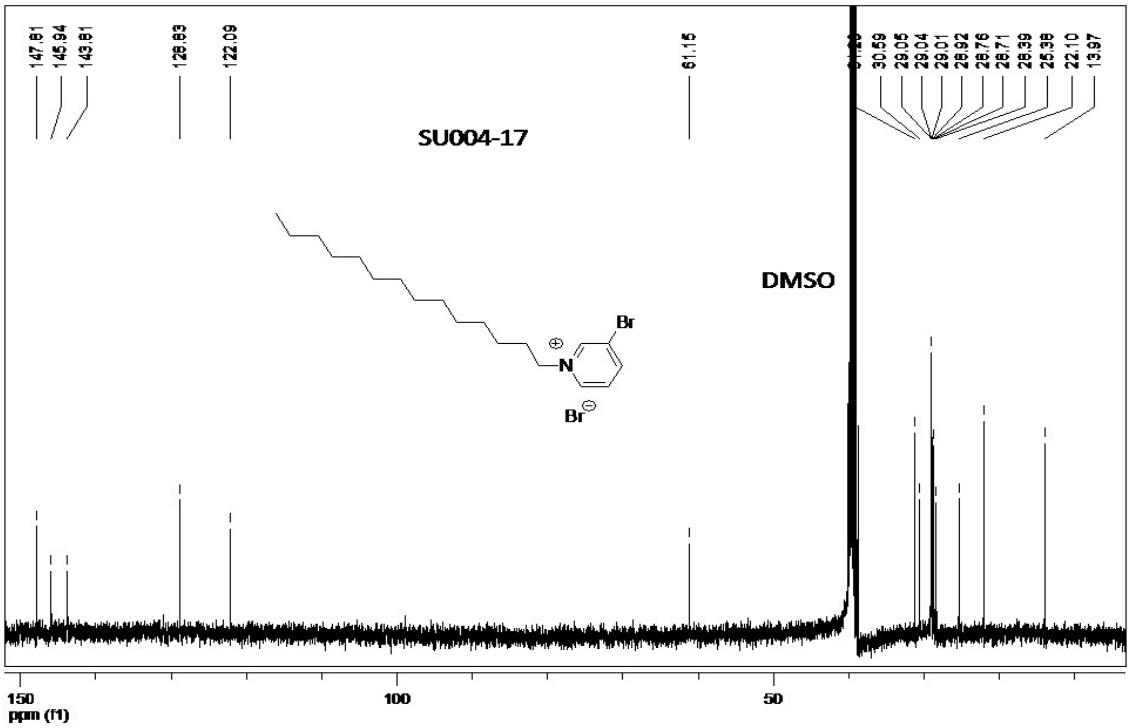


**Figure S7**. [13]C-NMR spectrum of **Py-Br-Br-14**.

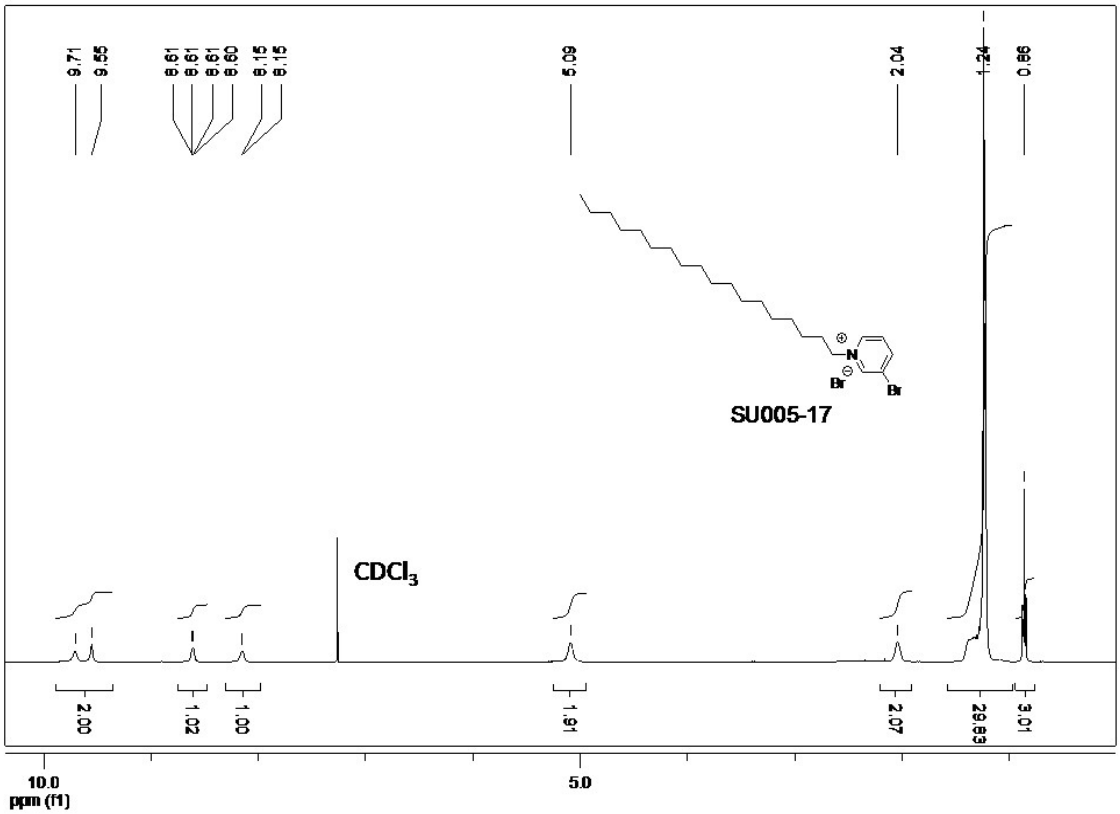


**Figure S8**. $^{1}$H-NMR spectrum of **Py-Br-Br-18**.

# 4. LIQUID CRYSTAL PROPERTIES

## 4.1 Thermogravimetric analysis (TGA)

TGA traces at a rate of 10 ºC min$^{-1}$ under a nitrogen atmosphere:

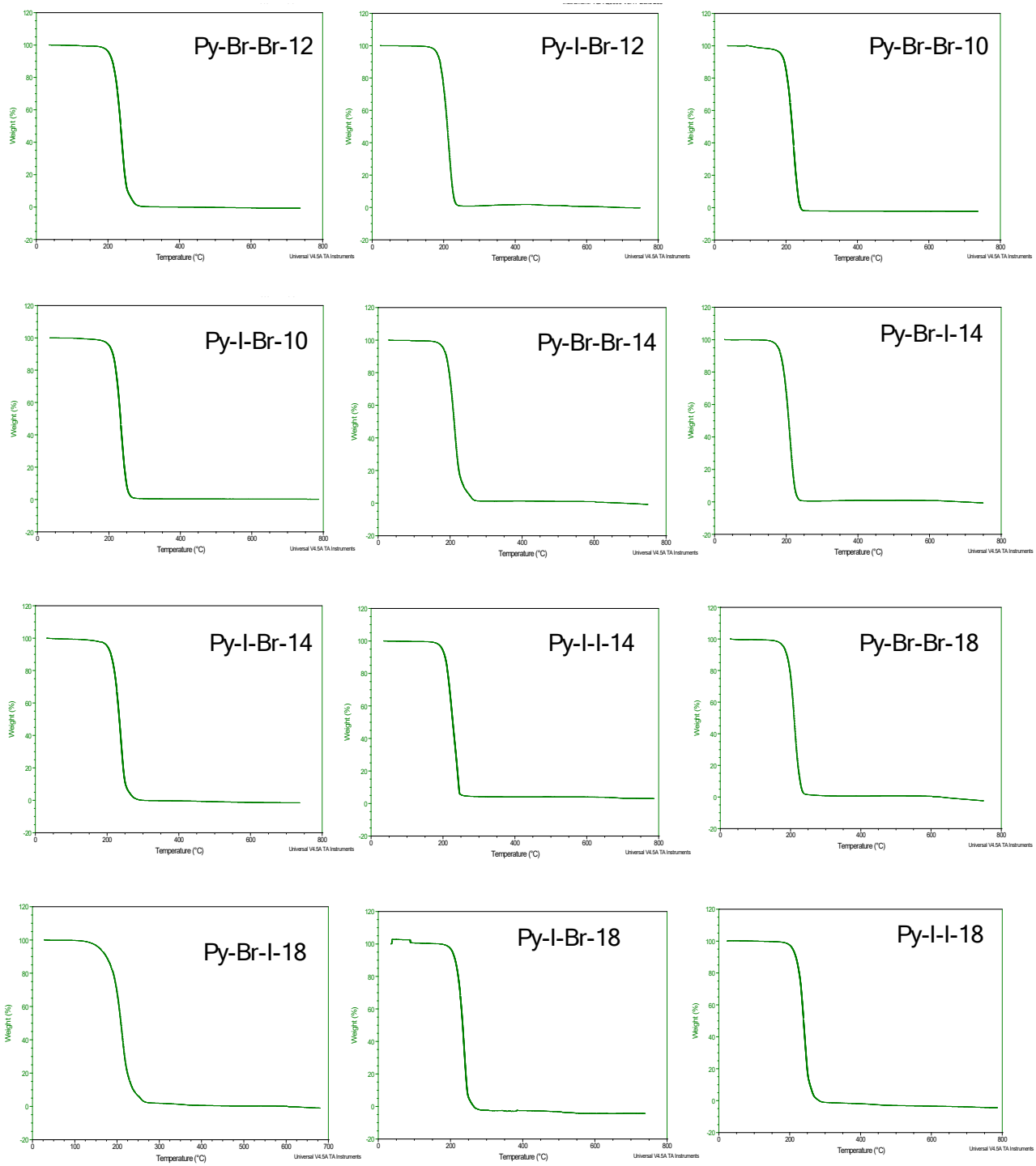

## 4.2 Differential scanning calorimetry (DSC)

DSC traces at a rate of 10 ºC min$^{-1}$ corresponding to the second heating scan (exo down):

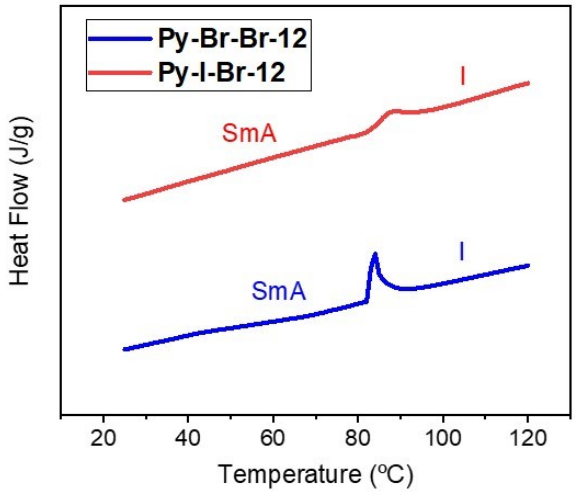


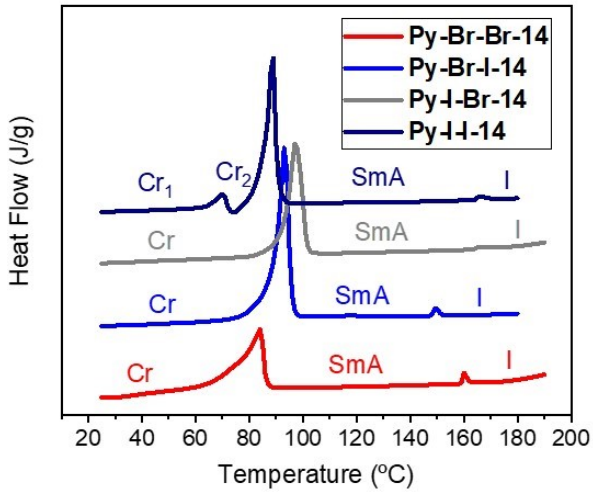


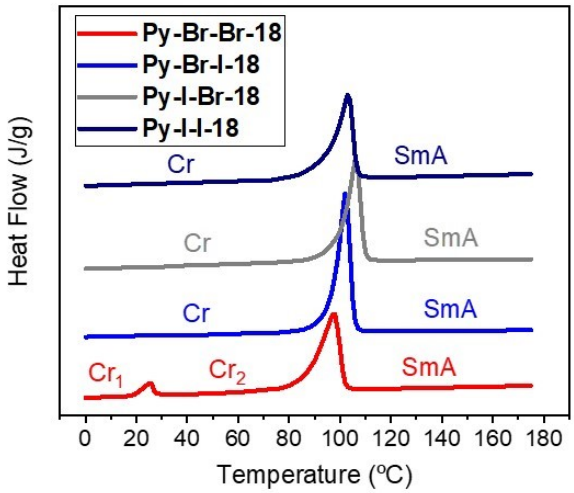

## 4.3 X-Ray diffraction (XRD)

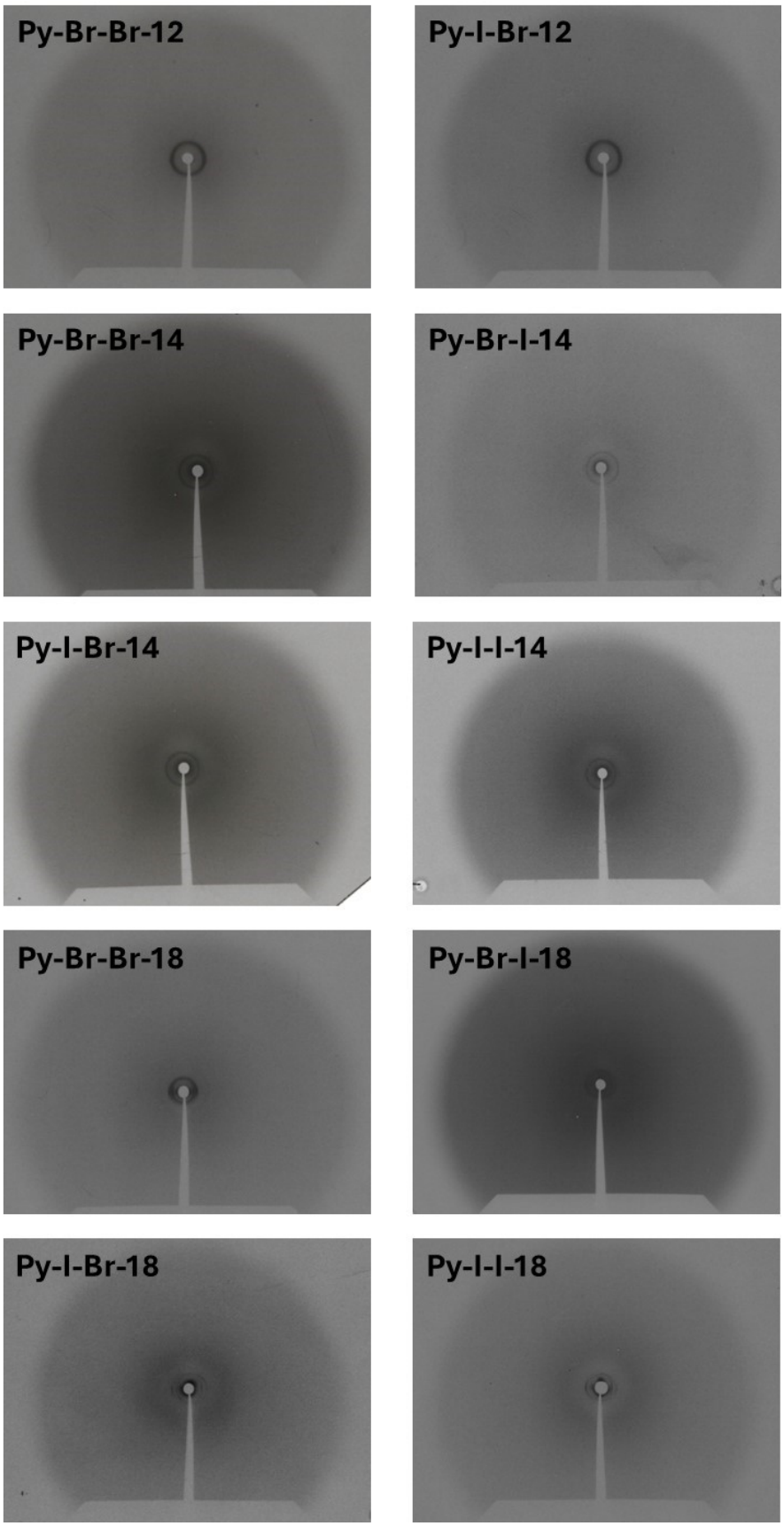

# 5 COMPUTATIONAL DETAILS

Density functional theory (DFT) calculations were carried out by using Gaussian09 package.[4] DFT with the B3LYP exchange–correlation functional[5–7] and Grimme D3BJ dispersion correction scheme[8,9] was utilized in conjunction with the 6-311$^{+}$G(d,p) basic set[10,11] was used for all of the atoms except halogen atoms, for which the DGDZVP basis set[12,13] was employed. The interaction energies between 3−halogen−pyridinium cations and halide anions ($\Delta E_{int}$) were calculated at the same level of theory as the difference between the total ionic pair and the sum of the total energies of the 3−halogen−pyridinium cation and halide anion. The interaction energies were corrected using the Boys–Bernardi counterpoise method in order to correct the basis set superposition error (BSSE)[14].

NCI analysis was performed using Multiwfn software[15]. A density cutoff of $\rho$ = 0.1 au was applied. Three-dimensional plots were created taking an isovalue of 0.4 for the reduced density gradient (s) and coloring in the [−0.050, 0.050] a.u. ±(λ2)ρ range using VMD software.[16]

**Table S5**. The interaction energies and the geometric parameters of optimized models using B3LYP−D3 and 6−311G+(d,p)/DGDZVP. The electron density multiplied by the sign of the second Hessian eigenvalue corresponding to the halogen bonding in the ion pairs [sign(λ2)ρ].

| **Ion pair** | **$\Delta E_{int}$ kJ/mol** | **d($X_1 \ldots X_2^-$) Å** | **<(C$X_1X_2$) degreee** | **rr[a]** | **sign($\lambda_2$)ρ a.u.** |
|---|---|---|---|---|---|
| **Py−Br−Br−1** 1-methyl-3-bromopiridinium bromide | -316.3 | 2.773 | 179.3 | 0.73 | -0.042 |
| **Py−Br−I−1** 1-methyl-3-bromopiridinium iodide | -294.2 | 3.015 | 179.2 | 0.75 | -0.034 |
| **Py−I−Br−1** 1-methyl-3-iodopiridinium bromide | -352.7 | 2.849 | 179.5 | 0.73 | -0.045 |
| **Py−I−I−1** 1-methyl-3-iodopiridinium iodide | -321.3 | 3.084 | 179.4 | 0.74 | -0.038 |

[a] Reduction ratio, rr = d($X_1 \ldots X_2^-$)/(RvdW($X_1$) + Rionic($X_2$)) where RvdW($X_1$) is the van der Waals radius of bromine (1.85 Å) or iodine (1.98 Å) and Rionic($X_2$) is the Pauling ionic radius of bromide (1.95 Å) or iodide (2.16 Å).

# 6 ELECTROCHEMICAL IMPEDANCE SPECTROSCOPY

Electrochemical impedance spectroscopy was carried out using a SI1260 Frequency Response Analyser (Schlumberger Instruments) over a frequency range of 1 Hz (some spectra from 0.1 Hz) to 1 MHz, with an applied AC voltage of 50 mV amplitude. The sample was placed inside a variable-temperature hot stage equipped with a Linkam TMS94 temperature controller. Conductivity measurements were performed as a function of temperature, ranging from 30 °C to the isotropic phase transition temperature, in 5 °C increments.

For cell preparation, an appropriate amount of the ionic liquid crystal was deposited onto one F-doped tin oxide (FTO, with 15 Ω $sq^{-1}$ sheet resistance) conducting glass substrate and then sandwiched with a second FTO electrode. The thickness was controlled using a thermoplastic sealing agent of 45 µm. The total electrode area, including the thermoplastic sealing, was approximately 2.2 $cm^2$, while the area covered by the conducting compound was around 0.25 $mm^2$. The assembled cell was heated to a few degrees above the melting point of the liquid crystal and gently pressed to form a uniform thin film. Following cell assembly, a random orientation of the mesophase was initially observed between the electrodes. Mechanical shearing was applied at the isotropic temperature to align the molecules, followed by slow cooling to room temperature at a rate of 0.05 °C·$min^{-1}$.

Impedance spectra were analyzed using complex-plane plots (imaginary component Z″ vs. real component Z′). The bulk resistance ($R_b$) was determined from the Z′ value at the minimum point between the high-frequency and low frequency semicircle or sloping line. Conductivity (σ, in S·$cm^{-1}$) was calculated using the formula: $\sigma = d/(Rb \cdot A)$, where d (cm) is the film thickness, A ($cm^2$) is the film area, and $R_b$ (Ω) is the bulk resistance of the sample.

Representative EIS spectra:

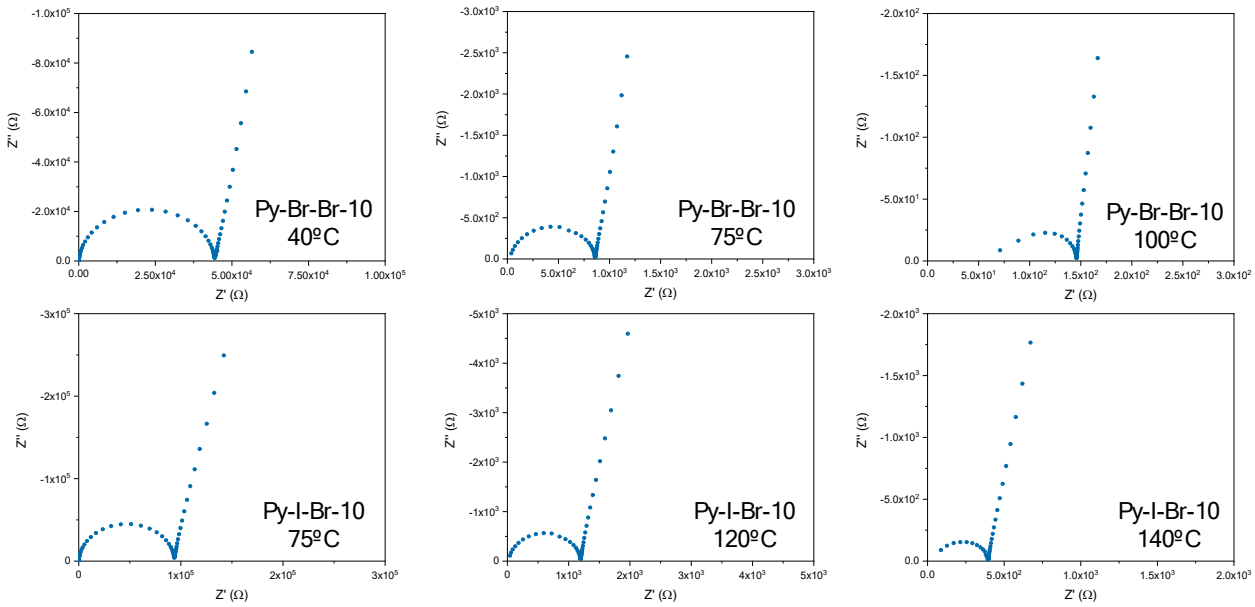

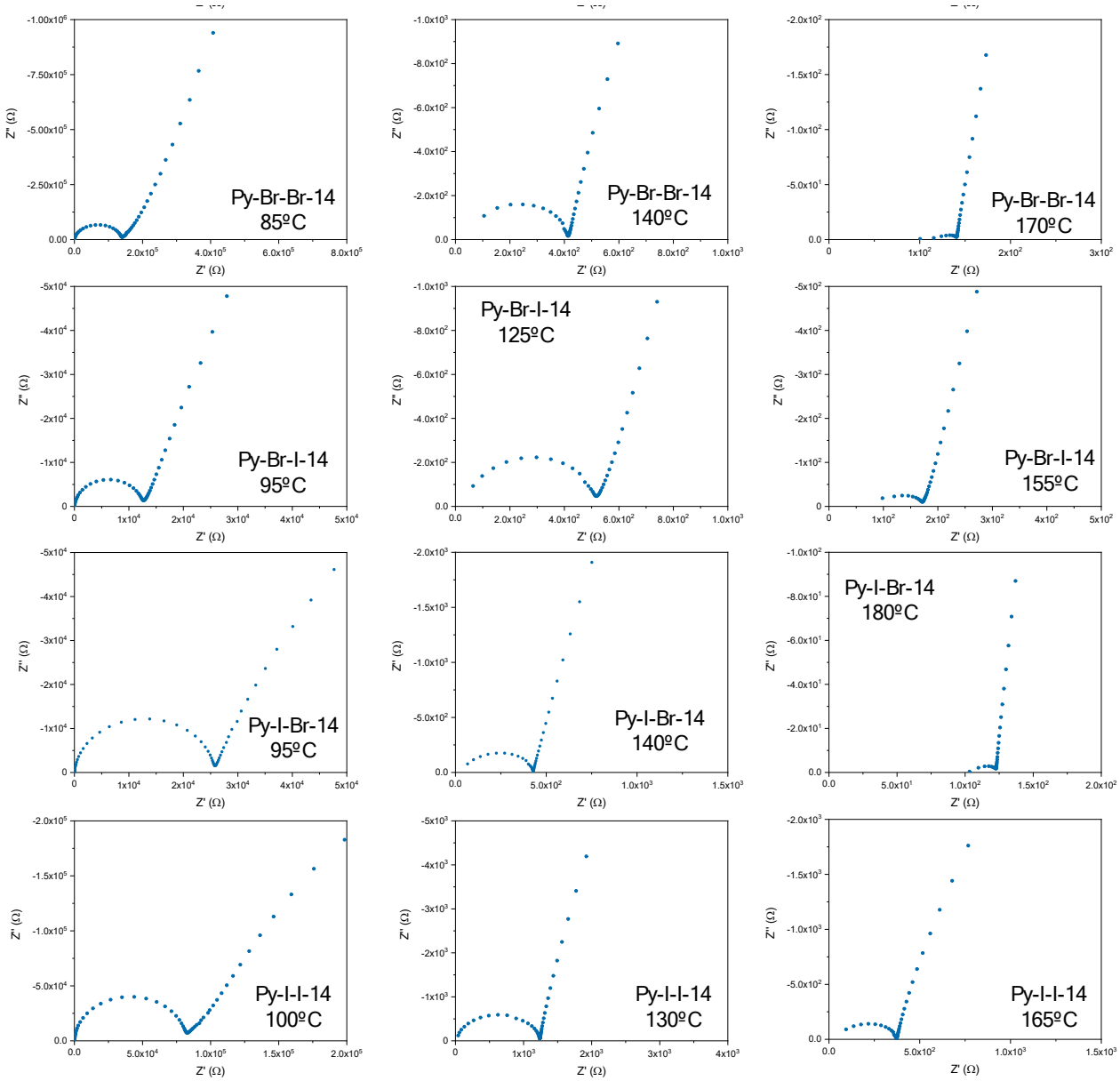
Py-Br-Br-14
85ºC
Py-Br-Br-14
140ºC
Py-Br-Br-14
170ºC
Py-Br-I-14
95ºC
Py-Br-I-14
125ºC
Py-Br-I-14
155ºC
Py-I-Br-14
95ºC
Py-I-Br-14
140ºC
Py-I-Br-14
180ºC
Py-I-I-14
100ºC
Py-I-I-14
130ºC
Py-I-I-14
165ºC
Z' (Ω)
Z'' (Ω)

# 7 SUPPLEMENTARY REFERENCES


(1) XSCANS. Siemens Analitycal X-Ray Instruments Inc.: Madison WI, 1994.

(2) Agilent (2014). CrysAlis PRO. Agilent Technologies Ltd, Yarnton, Oxfordshire, E. CrysAlis PRO.

(3) Sheldrick, G. M. Crystal Structure Refinement with SHELXL. *Acta Crystallogr. Sect. C Struct. Chem.* **2015**, *71*, 3–8. https://doi.org/10.1107/S2053229614024218.

(4) *Gaussian 09, Revision A.02*, M. J. Frisch, G. W. Trucks, H. B. Schlegel, G. E. Scuseria, M. A. Robb, J. R. Cheeseman, G. Scalmani, V. Barone, G. A. Petersson, H. Nakatsuji, X. Li, M. Caricato, A. Marenich, J. Bloino, B. G. Janesko, R. Gomperts, B. Mennucci, H. P. Hratchian, J. V. Ortiz, A. F. Izmaylov, J. L. Sonnenberg, D. Williams-Young, F. Ding, F. Lipparini, F. Egidi, J. Goings, B. Peng, A. Petrone, T. Henderson, D. Ranasinghe, V. G. Zakrzewski, J. Gao, N. Rega, G. Zheng, W. Liang, M. Hada, M. Ehara, K. Toyota, R. Fukuda, J. Hasegawa, M. Ishida, T. Nakajima, Y. Honda, O. Kitao, H. Nakai, T. Vreven, K. Throssell, J. A. Montgomery, Jr., J. E. Peralta, F. Ogliaro, M. Bearpark, J. J. Heyd, E. Brothers, K. N. Kudin, V. N. Staroverov, T. Keith, R. Kobayashi, J. Normand, K. Raghavachari, A. Rendell, J. C. Burant, S. S. Iyengar, J. Tomasi, M. Cossi, J. M. Millam, M. Klene, C. Adamo, R. Cammi, J. W. Ochterski, R. L. Martin, K. Morokuma, O. Farkas, J. B. Foresman, and D. J. Fox, Gaussian, Inc., Wallingford CT, **2016**.

(5) Lee, C. T.; Yang, W. T.; Parr, R. G. Development of the Colle-Salvetti Correlation-Energy Formula into a Functional of the Electron-Density. *Phys. Rev. B* **1988**, *37* (2), 785–789. https://doi.org/10.1103/PhysRevB.37.785.

(6) Becke, A. D. Density-Functional Thermochemistry .III. The Role of Exact Exchange. *J. Chem. Phys.* **1993**, *98* (7), 5648–5652. https://doi.org/10.1063/1.464913.

(7) Becke, A. D. A New Mixing of Hartree-Fock and Local Density-Functional Theories. *J. Chem. Phys.* **1993**, *98* (2), 1372–1377. https://doi.org/10.1063/1.464304.

(8) Grimme, S.; Antony, J.; Ehrlich, S.; Krieg, H. A Consistent and Accurate Ab Initio Parametrization of Density Functional Dispersion Correction (DFT-D) for the 94 Elements H-Pu. *J. Chem. Phys.* **2010**, *132* (15), 154104. https://doi.org/doi:http://dx.doi.org/10.1063/1.3382344.

(9) Grimme, S.; Ehrlich, S.; Goerigk, L. Effect of the Damping Function in Dispersion Corrected Density Functional Theory. *J. Comput. Chem.* **2011**, *32* (7), 1456–1465. https://doi.org/10.1002/jcc.21759.

(10) Krishnan, R.; Binkley, J. S.; Seeger, R.; Pople, J. A. Self-Consistent Molecular Orbital Methods. XX. A Basis Set for Correlated Wave Functions. *J. Chem. Phys.* **1980**, *72* (1), 650–654. https://doi.org/10.1063/1.438955.

(11) Clark, T.; Chandrasekhar, J.; Spitznagel, G. W.; Schleyer, P. V. R. Efficient Diffuse Function-augmented Basis Sets for Anion Calculations. III.* The 3-21+G Basis Set for First-row Elements, Li–F. *J Comp Chem* **1983**, *4*, 294–301.

(12) Sosa, C.; Andzelm, J.; Elkin, B. C.; Wimmer, E.; Dobbs, K. D.; Dixon, D. A. A Local Density Functional Study of the Structure and Vibrational Frequencies of Molecular Transition-Metal Compounds. *J. Phys. Chem.* **1992**, *96* (16), 6630–6636. https://doi.org/10.1021/j100195a022.

(13) Godbout, N.; Salahub, D. R.; Andzelm, J.; Wimmer, E. Optimization of Gaussian-Type Basis-Sets for Local Spin-Density Functional Calculations. 1. Boron through Neon, Optimization Technique and Validaiton. *Can. J. Chem.* **1992**, *70* (2), 560–571. https://doi.org/10.1139/v92-079.

(14) Boys, S. F.; Bernardi, F. The Calculation of Small Molecular Interactions by the Differences of Separate Total Energies. Some Procedures with Reduced Errors. *Mol. Phys.* **1970**, *19* (4), 553–566. https://doi.org/10.1080/00268977000101561.

(15) Lu, T.; Chen, F. Multiwfn: A Multifunctional Wavefunction Analyzer. *J. Comput. Chem.* **2012**, *33* (5), 580–592.

https://doi.org/10.1002/jcc.22885.

(16) Humphrey, W.; Dalke, A.; Schulten, K. VMD: Visual Molecular Dynamics. *J. Mol. Graph. Model.* **1996**, *14* (1), 33–38. https://doi.org/10.1016/0263-7855(96)00018-5.